Surface Charge Density and Electrokinetic Potential of Highly Charged Minerals: Experiments and Monte Carlo Simulations on Calcium Silicate Hydrate

Christophe Labbez,*,† Bo Jönsson,‡ Isabelle Pochard,† André Nonat,† and Bernard Cabane§

LRRS, UMR CNRS 5613, Université de Bourgogne, F-21078 Dijon Cedex, France, Theoretical Chemistry, Chemical Center, POB 124, S-221 00 Lund, Sweden, and PMMH, ESPCI, 10 rue Vauquelin, F-75231 Paris Cedex 05, France

Received: December 6, 2005; In Final Form: March 14, 2006

In this paper, we are concerned with the charging and electrokinetic behavior of colloidal particles exhibiting a high surface charge in the alkaline pH range. For such particles, a theoretical approach has been developed in the framework of the primitive model. The charging and electrokinetic behavior of the particles are determined by the use of a Monte Carlo simulation in a grand canonical ensemble and compared with those obtained through the mean field theory. One of the most common colloidal particles has been chosen to test our theoretical approach. That is calcium silicate hydrate (C−S−H) which is the main component of hydrated cement and is known for being responsible for cement cohesion partly due to its unusually high surface charge density. Various experimental techniques have been used to determine its surface charge and electrokinetic potential. The experimental and simulated results are in excellent agreement over a wide range of electrostatic coupling, from a weakly charged surface in contact with a reservoir containing monovalent ions to a highly charged one in contact with a reservoir with divalent ions. The electrophoretic measurements show a charge reversal of the C−S−H particles at high pH and/or high calcium concentration in excellent agreement with simulation predictions. Finally, both simulation and experimental results clearly demonstrate that the mean field theory fails not only quantitatively but also qualitatively to describe a C−S−H dispersion under realistic conditions.

1. Introduction

Most minerals develop a charge at their surface when they are immersed in an aqueous solution. Simultaneously, due to electrostatic interactions and thermal agitation, solvated ions accumulate at the mineral/solution interface and form an ionic cloud, called the electric double layer (EDL), which, at equilibrium, balances the mineral surface charge. The electrostatic interactions in the EDL control many properties of mineral surfaces as well as the interactions between them: phase equilibria, coagulation, aggregation, sedimentation, filtration, catalysis reaction, and ionic transport in porous media. An understanding and an accurate modeling of the mineral/solution interfaces are, thus, of paramount importance from a practical point of view.

The most commonly used model to describe the EDL is the primitive model (PM) where the ions are modeled as charged hard spheres; the solvent is treated as a dielectric continuum, and solid surfaces are assumed to be smooth and uniformly charged. The mean field approximation of the PM based on the Poisson−Boltzmann equation (PB) is the most used theory in that area. In this approach, ions are assumed to be point charges and are interacting with the surface and the surrounding electrolyte solution through an average electrostatic potential. As a consequence, the many-body effects due to interactions between the charged particles (electrostatic and hard-core correlations) are left out. Despite these approximations, the mean field theory is able to catch the main features of the EDL for electrolyte solutions containing monovalent ions at low concentration next to a weakly charged solid surface. For a highly coupled system (high concentration, multivalent ions, and high surface charge) and in particular for mineral surfaces presenting a high surface charge density, however, the neglect of ion−ion correlations leads to quantitatively and qualitatively wrong results.

For instance, nonclassical phenomena (not predict by the mean field theory) such as the apparent charge reversal[1−9] and the appearance of attractive interactions between equally charged surfaces[10−12] in EDL theory can occur. Both the charge reversal and the attraction between equally charged particles are generated by ion−ion correlations, but while the latter is robust the charge reversal seems to be a more transitory phenomenon.[24] Such phenomena have been reported through experiments,[13−21] accurate theories,[2,4−8,11−12,14,22] and simulations[1,3,9,10,12,23,24] during the two past decades. The reader interested in this matter is also referred to recent reviews.[25,26] However, an accurate theoretical approach of a mineral charging process which includes the ion−ion correlations is still lacking. We shall present in this paper such an approach applied to highly charged minerals in the alkaline pH range for which the charging and electrokinetic behavior is studied through Monte Carlo simulations in the framework of the PM.

Another point of particular interest in this work is the comparison between the results of our simulations and various experiments conducted on one of the most common highly charged colloidal particles. That is calcium silicate hydrate (C−S−H[27]) which is the major constituent (60%) of hydrated

* To whom correspondence should be addressed. E-mail: Christophe.labbez@u-bourgogne.fr.
† Université de Bourgogne.
‡ Chemical Center.
§ ESPCI.

10.1021/jp057096+ CCC: $33.50
Published on Web 04/13/2006

cement. These particles are formed through the conjugated reactions of dissolution of tricalcium silicate grains (C_3S[27]) and of precipitation when the supersaturation is reached. C−S−H particles are in the form of nanoplatelets with dimensions 60 nm × 30 nm × 5 nm. A typical cement paste has a very high pH, and the C−S−H nanoparticles become highly negatively charged due to titrating silanol groups. This negative surface charge is counterbalanced mainly by divalent calcium counterions in the solution. Recently, we have described the forces between such particles and how they are affected by the addition of different salts to the cement paste.[19,23,24] It appears that the aggregation of the negatively charged C−S−H particles ensuring the cohesion of the final material is driven by attractive ion−ion correlations,[10,12] which become predominant in the presence of calcium counterions and the high surface charge density of the particles. The general conclusion from this work is that the cohesion of cement is very robust provided that the surface charge density of the particles and/or the concentration of Ca^{2+} is high. In previous studies, we have assumed (guessed) a reasonable surface charge density in an ad hoc fashion and kept it fixed. This is not a completely satisfactory situation. A more realistic approach would be to set the pH of the solution and then let the external conditions, that is, salt concentration, paste concentration, and so forth, determine the surface charge density. This is the route we will follow in the present study.

The negative charge of the C−S−H particles, as is also the case for the original C_3S grains, comes from titrating silanol groups on their surface

$$-\mathrm{Si}-\mathrm{OH} \leftrightarrow -\mathrm{Si}-\mathrm{O}^- + \mathrm{H}^+ \tag{1}$$

The surface intrinsic dissociation constant (K_0) corresponding to this reaction, from which the fraction of ionized groups (α) at equilibrium is obtained, can be expressed as

$$K_0 = \frac{a_{\mathrm{Si-O}} a_{\mathrm{H}}}{a_{\mathrm{Si-OH}}} \tag{2}$$

where $a_{\mathrm{Si-O}}$ and $a_{\mathrm{Si-OH}}$ are the surface activities of ionized and neutral sites, respectively, and a_{H} is the activity of the proton which fixes the pH value.

The exact structure of the C−S−H platelets is not known, but it is generally accepted that it is close to that of another mineral, tobermorite.[28−30] By accepting this view, we can calculate the number of surface silanols to 4.8/nm^2. The first dissociation constant for silicic acid

$$\mathrm{H_4SiO_4} \leftrightarrow \mathrm{H_3SiO_4}^- + \mathrm{H}^+ \tag{3}$$

has a $pK_0 = 9.8$. The second, third, and so forth, dissociation constants are not well-known due to the formation multinuclear silicate complexes.[31,32]

A surface with densely packed titrating groups will lead to a complex and extended titration curve. That is, while a single isolated acidic group with a $pK_0 = 9.8$ would be dissociated to 90% at pH = 10.8, the corresponding surface site on a C−S−H particle would only be dissociated to about 10% due to the repulsion between the ionized sites. This is normally referred to as a "polyelectrolyte effect". One consequence of this is that an increase in the number of surface sites does not necessarily lead to an equally large increase in the surface charge density at a given pH. The titration behavior of polyelectrolytes of various geometries[33,34] as well as mineral surfaces[35−38] has in the past been described with a variety of mean field approximations based on the dielectric continuum model. Within this theory, one obtains the result that the titration curve of a mineral surface is a superposition of the curves for the individual groups: the fraction of dissociated group of any type being given by the relation

$$\mathrm{pH} - \log\frac{\alpha}{1-\alpha} = \mathrm{p}K_0 - \frac{1}{2.303kT} e\Psi(0) \tag{4}$$

where e is the elementary charge, k the Boltzmann constant, T the temperature, and $\Psi(0)$ the average surface potential calculated through the PB equation. The dielectric continuum model seems to capture the essential physics of the system, but it has to be solved in a more accurate way than what the mean field approximation offers. For weakly charged surfaces in the presence of only monovalent counterions, the mean field might be appropriate, but with highly charged solid surfaces and in particular with divalent counterions, it could predict qualitatively wrong results.

A number of factors determine the titration characteristics of mineral surfaces. These include site density of titratable groups, salt concentration and valency, suspension concentration (in the case of colloidal particles) as well as the amount of other charged additives. It is the aim of the present study to describe the titration behavior of mineral surfaces taking C−S−H particles as an example, in equilibrium with a bulk solution of varying conditions, combining accurate Monte Carlo simulations with experimental techniques. In particular, the evolution of surface charge as well as the electrokinetic potential of C−S−H against solutions containing the common ions Na^+, Ca^{2+}, SO_4^{2-}, PO_4^{3-}, OH^-, and Cl^- are studied. The Monte Carlo (MC) simulations will focus on the electrostatic interactions alone, and any chemical specific interactions will be neglected. This approach captures the main physics for highly charged systems and provides a coherent and transparent picture of the system. We note, consequently, that many of the conclusions regarding the titration and electrokinetic properties of C−S−H are also valid for C_3S or, potentially, any other highly charged surface.

2. Materials and Methods

2.1. Experiments. 2.1.1. C−S−H Suspensions Preparation. The C−S−H mother suspension has been prepared by mixing 5.946 g of analytical grade calcium oxide (Prolabo), 9.724 g of colloidal silica TA92 (Rhodia), and 791.50 g of distilled−deionized milli-Q water. These proportions have been chosen to obtain C−S−H of a Ca/Si stoichiometric ratio equal to 0.66. The calcium oxide powder has been decarbonated in a furnace at 1000 °C for 4 h. The milli-Q water has been boiled to remove soluble CO_2. Silica has not undergone any treatment. The pH of the obtained suspension is 10.35, and the liquid-to-solid ratio is 50.0. For the titration experiment, this suspension has been used as is while it has been diluted a hundred times for the electrokinetic measurements.

2.1.2. Surface Charge Titration. Various batches of pure C−S−H suspensions were prepared, all having similar properties, that is, a liquid-to-solid ratio of 50.0 (in weight) and a volume of 35.0 mL. These were obtained from the same initial pure C−S−H suspension whose preparation protocol is described above. Two freshly prepared 1 and 5 M NaOH basic solutions were used to titrate the C−S−H suspensions depending on which final pH is supposed to be reached: 1 M for pH < 12.5 and 5 M for pH ≥ 12.5. It allows us to limit the dilution of the suspension during the titration experiment. All solutions were prepared from milli-Q quality water (conductivity <1 μS at room temperature).

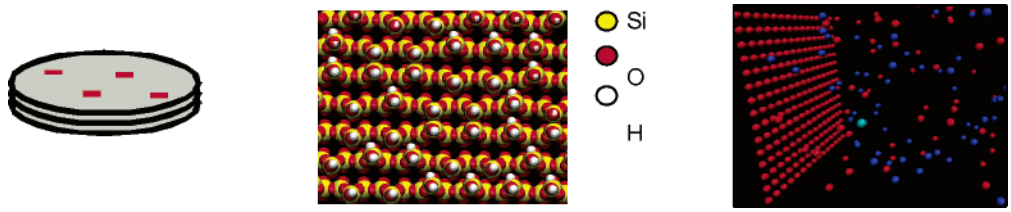

Figure 1. (a) Schematic representation of the lamellar structure of a C−S−H crystallite. Typical dimensions are 30 × 60 × 5 nm^3. Each sheet of the C−S−H crystallite is composed of two planes of calcium covered by parallel silicate chains. (b) Detailed structure of the tobermorite surface which is thought to be close to that of C−S−H. One could distinctly observe the parallel silicate chains with silanol groups generating the surface charge. (c) A slab model of one C−S−H particle in contact with a salt solution. Titrating sites, modeling silanol groups of the C−S−H surface, are treated as discrete and distributed on a square lattice of dimensions 4.56 × 4.56 Å^2. Sites are allowed to titrate according to the solution pH and composition.

Titration experiments with C−S−H suspensions were carried out between pH 10.35, the initial pH of our suspension, and 13.5. This pH range is imposed by the fact that C−S−H does not exist below a pH value of 10 as discussed below. Care has been taken to prevent contamination of solutions with CO_2. Blank solutions, having the same volume as batches used for the titration experiments, were prepared to correct for minor CO_2 contamination. These were obtained from the supernatant of the initial suspension after centrifugation and filtration on a 0.22 μm Millipore apparatus. The experiments were conducted by adding a known amount of base to both blank solutions and suspensions. Blank solutions and C−S−H suspensions were then aged and vigorously shaken during a 3 week period to ensure a good equilibration. Subsequently, the suspensions were centrifuged in a high-speed centrifuge at 9000 rpm from which the supernatant solutions were taken. Minor contamination with CO_2 in this procedure cannot be completely precluded. Finally, the pH value and sodium and calcium content of both blank and supernatant solutions of C−S−H suspensions were measured with a suitable high alkalinity pH electrode and inductively coupled plasma absorption optical spectroscopy, respectively. The resulting excess amount of sodium (Na^{ex}) incorporated in the EDL, the portion of sodium ions neutralizing the surface charge, and consumption of hydroxide ions have then been deduced from subtracting the total content of sodium and hydroxide remaining in suspensions from that of blank solutions. The excess concentration of an ion (c_i^{ex}), from which the excess amount is obtained, is defined as the difference between its bulk (c_i^0) and EDL concentrations (c_i^{DL})

$$c_i^{ex} = c_i^{DL} - c_i^0 \tag{5}$$

It is often difficult to properly determine the total specific surface area when analyzing surface titration experiments. We have tried to overcome this problem by determining the total number of titrating surface sites (silanols) of our C−S−H suspensions from the known mass of reactant used to synthesize the C−S−H and stoichiometric considerations. On average, there are two −OH functions per three silicium atoms from the known structure and composition of C−S−H synthesized. We consider all silanol groups as identical, that is, no distinction is made between titrating sites situated at the inner or outer surfaces of C−S−H crystallites; see parts a and b of Figure 1.

In the $CaO-SiO_2-H_2O$ system, the invariant point[39] where silica and C−S−H coexist corresponds to pH ∼ 10. As a consequence, C−S−H exists only at pH values higher than 10, and C−S−H nanoparticles do not possess a point of zero charge. Our titration experiments then only give the net increase of the negative surface charge as pH is increased. The surface charge corresponding to the solution pH from which the experiments start and hence the complete surface charge titration cannot be determined by experiments alone.

2.1.3. Electrophoretic Mobility. The electrokinetic potential of C−S−H particles was measured by electrophoresis. C−S−H suspensions used for mobility measurements were similar to those used for the titration experiments, except that the liquid-to-solid ratio used for electrophoresis was 5000 in weight. The apparatus used for the determination of the electrokinetic properties of C−S−H suspension was a COULTER DELSA 440. The electrophoretic mobility is measured through the Doppler shift of the laser light scattered by the particles during electrophoresis. Granulometric measurements of the suspensions used to characterize the ζ potential of C−S−H particles have shown that their size is generally a factor of 50−100 bigger than the size of the individual C−S−H crystallites.[20] Thus, we are led to conclude that in reality we measure the mobility of agglomerates, composed of many individual crystallites. These agglomerates have an effective size on the order of several hundred nanometers. Assuming that an agglomerate can be modeled as a spherical particle with impermeable and smooth surfaces with a much larger size than the extension of the EDL, then the Smoluchowski equation can be used to estimate the electrokinetic potential from the electrophoretic mobility[40]

$$\zeta \approx \eta \mu_E / \epsilon_r \tag{6}$$

where ζ is the electrokinetic potential and η the viscosity of the solvent.

2.2. Model. 2.2.1. C−S−H. The crystal structure of C−S−H is known to be close to that of tobermorite as confirmed by NMR,[28,29] X-ray diffraction, and more recently by AFM[30] and molecular simulations.[41] However, the exact structure of C−S−H is still undetermined. Lacking detailed information on the geometry of C−S−H nanoparticles and for simplicity reasons, a lattice model of ionizable sites on the water/solid interface is applied. The C−S−H nanoparticles are represented by their surface modeled as an infinite planar wall, with discrete surface sites regularly distributed on a square lattice; see Figure 1c. To reach the known surface silanol group density (∼4.8 sites/nm^2), the lattice parameter was chosen to be 4.56 Å. To further simplify the model, it is assumed that the surface sites present at the C−S−H surface are pointlike groups which are given a neutral charge when protonated and a charge of −1 when deprotonated, according to the solution pH. The C−S−H surface is put in contact with an electrolyte solution in a parallelepipedic cell forming a slab; see Figure 1c. The simulation box, which is overall electroneutral, is then composed of one C−S−H particle in contact with a salt solution. The concentration of the latter is imposed by the equilibrium with a bulk in a grand canonical procedure. The system is assumed to be infinite (periodic boundary conditions are applied) in the

two dimensions parallel to the surface and finite in the other one. That is, in the perpendicular direction, the cell is closed by the C−S−H surface on the left and a neutral impenetrable wall on the right.

2.2.2. Ionic Solution and Interactions. The electrolyte solution is described in the framework of the so-called primitive model, that is, ions are charged hard spheres and water is implicitly represented by a relative dielectric permittivity, $\epsilon_r = 78.5$ (at 298 K), which is assumed to be constant throughout space. The interaction energy between two charged species i and j is expressed by

$$u(r_{ij}) = z_i z_j e^2/4\pi\epsilon_0\epsilon_r r_{ij} \quad r > (d_i + d_j)/2 \tag{7a}$$

$$u(r_{ij}) = \infty \quad r \le (d_i + d_j)/2 \tag{7b}$$

where z is a valency, e is the elementary charge, ϵ_0 is the permittivity of free space, d the hard-core diameter, and r_{ij} the distance between particles i and j. The radii of co- and counterions are set equal and chosen to be 2 Å for all salt solutions studied to maintain a simple model. Previous analysis of seawater indicates that the appropriate variation of ion radii is rather limited.[42] It is a reasonable choice that will be shown later in this paper when studying the electrokinetic potential.

2.2.3. Monte Carlo Simulations. Monte Carlo simulations were performed in the grand canonical ensemble[43] (GCMC) with use of the traditional Metropolis Monte Carlo procedure.[44] In other words, the chemical potential of ionic species contained in the simulation box are equilibrated with those of an infinite bulk solution; see ref 24 for a detailed presentation of the procedure. The chemical potentials are initially calculated by performing simulation of a bulk solution of the desired ionic concentration and composition using a modified Widom method[45,46] in the canonical ensemble. The accuracy of the dimensionless chemical potential (μ/kT) of ionic species is better than ±0.005. The temperature is kept equal to 298 K.

The dimensions of the C−S−H surface were always larger than 100 × 100 Å^2 ensuring a total number of sites higher than 400. The third dimension of the simulation box was scaled accordingly, but was never less than 100 Å, imposing a number of ions larger than 300, and chosen large enough so that the properties of EDL at the C−S−H surface were unaffected by the abrupt truncation of the system by the neutral closing wall. The latter condition implies that a homogeneous fluid, with the bulk properties, exists in the middle of the simulation cell. The convergence of the properties of EDL at the C−S−H surface were controlled for some of the cases studied by doubling the cell dimensions and/or by replacing the neutral closing wall by a second C−S−H surface. A total of 10^5 moves per mobile particle were attempted in each GCMC run. Simulations were conducted for a surface having a site density of 4.8 sites/nm^2 and sites of $pK_0 = 9.8$. These numbers are the standard value unless otherwise stated. A method, introduced simultaneously by Torrie and Valleau[47] and Jönsson et al.[50] and also described in our previous paper,[24] the so-called charged sheet method, is used to treat the long-range contributions of the Coulombic energy.

2.2.4. Surface Charge Titration. The surface sites are initially protonated and the initial configuration of the C−S−H surface is uncharged. During the simulation, after every 5th attempted move of the mobile charges, an attempt was also made to delete or add a proton on a titrating site. Protons are not explicitly treated. Instead, a negative elementary charge is assigned to the titrating site as it is deprotonated. The opposite procedure takes place when a site is protonated. To satisfy the cell electroneutrality when adding one negative charge to a surface site, a hydroxide ion is deleted from the solution. Alternatively, one could instead add a positive ion, but our choice for this particular application is more in line with the corresponding experimental procedure. The trial energy for the protonation or deprotonation of a particular silanol group can be formulated[48] as

$$\Delta U = \Delta U_{el} + kT \ln 10(\mathrm{pH} - \mathrm{p}K_0) \quad \text{for protonation} \tag{8a}$$

$$\Delta U = \Delta U_{el} - kT \ln 10(\mathrm{pH} - \mathrm{p}K_0) \quad \text{for deprotonation} \tag{8b}$$

where ΔU_{el} is the change in electrostatic free energy due to the addition and deletion of charges and pK_0 is the negative decimal logarithm of the intrinsic dissociation constant (K_0) for the model compound. What we mean by intrinsic dissociation constant is the one that we would get from one single, isolated site. A pK_0 value of 9.8 was assigned to the silanol groups which is equal to that of the first deprotonation reaction of silicic acid. Here, we assume that the Gibbs free energy change due to, for example, hydration and ligand binding is relatively invariant over, on one hand, the salt concentrations studied and on the other hand, the structural and chemical changes between silicic acid and C−S−H nanoparticle. In this approximation, the only contribution to the shift of the apparent pK of C−S−H surface sites, the pH value at which half of the silanol groups are ionized, is the difference in electrostatic free energy between systems of fully protonated and deprotonated sites. Thus, we are only concerned by electrostatic interactions as given by eq 8. The ionization state of a surface can be conveniently described by the dimensionless surface ionization fraction (α) that is defined by the surface charge density (σ_0) to surface site density (ρ_N) ratio

$$\alpha = \sigma_0/\rho_N F \tag{9}$$

where F is the Faraday constant. The surface ionization fraction is calculated with an accuracy better than ±0.01. One should note that α is unaffected by the way the simulation cell is closed in the normal direction, that is, by a neutral wall or a second C−S−H surface, as long as the two EDLs are not interacting. (In a later paper, we shall investigate a system in which two EDLs are interacting, namely, the so-called charge regulation.)

2.2.5. Electrostatic and Electrokinetic Potential. One can calculate the surface potential and the complete electric potential profile in the double layer by integrating the Poisson equation twice. That yields

$$\Phi(x) = -e/\epsilon_0\epsilon_r \cdot \sum_i q_i \int_x^\infty (t - x)\rho_i(t)\, \mathrm{d}t \tag{10}$$

where ρ_i is the ion density of the bulk solution. A more general expression for the potential profile in the EDL for nonidentical ion size can be found in ref 49.

The surface potential is generally not accessible experimentally. Instead, we can only approximate the electrostatic potential of the "diffuse" part of the EDL by the so-called electrokinetic (ζ) or ζ potential.[40] This latter is generally assumed to be equal to the "diffuse potential". Since, in our simulations, ions are allowed to penetrate the surface water layer, a shift of one and half ion diameter (6 Å) per surface is assumed for the location of the plane separating the "dense" to the diffuse part of the EDL and thus for the plane where the ζ potential is thought to be measured. This assumption is a weak point when comparing simulation results with experimental ones.

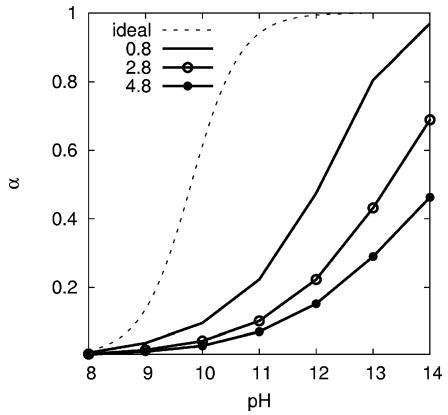

Figure 2. Simulated (GCMC) ionization fraction, α, vs pH for increasing surface site density: 0.8 (solid line), 2.8 (solid line, empty circles), and 4.8 sites/nm^2 (solid line, filled circles). The ideal curve corresponding to noninteracting sites (dashed line) is given for comparison. The surface is in equilibrium with a bulk solution containing 2 mM NaX.

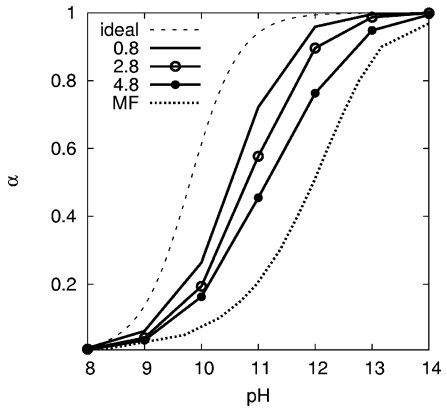

Figure 3. Simulated (GCMC) ionization fraction, α, vs pH for increasing surface site density: 0.8 (solid line), 2.8 (solid line, empty circles), and 4.8 sites/nm^2 (solid line, filled circles). The mean field curve for 4.8 sites/nm^2 (dotted line) and the ideal curve (dashed line) are given for comparison. The surface is in equilibrium with a bulk solution containing 2 mM CaX_2.

As discussed in ref 52, for calculating the potential profile and hence ζ from eq 10, a cutoff distance of $x = L_c$ from the charged surface has been chosen with the requirement that at L_c the bulk properties are recovered, that is, $\sum z_i\rho_i = 0$. Small differences have been found for the calculated values of ζ when replacing the neutral closing wall by a second C−S−H surface and/or by changing L_c, but they are within the statistical uncertainty (±1 mV). A more accurate method to calculate Φ(x) and hence ζ has been purposed by Torrie and Valleau; see ref 48. However, the statistical uncertainty of the chosen method is small enough when compared with the typical experimental uncertainties of electrokinetic measurements.

3. Results and Discussion

3.1. Surface Charge Titration. Before comparing the simulation and experimental results on surface charge titration, let us introduce some simulation data. First of all, some general behaviors already found with the classical surface charge titration models in the framework of the mean field theory, such as 1-p*K*, 2-p*K*, and MUSIC models,[35−37] are briefly presented. Then, a breakdown of the classical theory under the present experimental conditions is pointed out.

3.1.1. Simulation Results. Figure 2 shows the dependence of the surface ionization fraction (α) for various surface site densities for a surface in equilibrium with a bulk solution containing 2 mM sodium 1:1 electrolyte. Because the Coulombic interaction between deprotonated groups is repulsive, α is smaller than in the ideal case and it decreases when the surface site density increases. Consequently, the apparent p*K* for the protonation of surface silanol groups is significantly shifted toward higher pH values when the surface site density reaches that of C−S−H particles; several pH units in this case.

When the monovalent sodium counterions are replaced by divalent calcium ones, then the shift of the apparent p*K* is greatly reduced. This is illustrated in Figure 3. Indeed, the screening gain, by exchanging monovalent by divalent counterions in the bulk, allows, at pH 14, the complete ionization of surfaces even for a surface site density of 4.8/nm^2 where only 50% of the sites are ionized for sodium salt.

The mean field theory qualitatively gives the same result, see Figure 3, but it largely underestimates the surface charge at high pH values. This failure is a direct consequence of the neglect of ion−ion correlation in the PB equation, which results in an underestimate of the accumulation of divalent calcium ions close to the charged surface. In some cases, this accumulation may lead to an *apparent* charge reversal; see refs 23 and 24 and below. It is common practice to introduce a specific binding between surface sites and calcium to account for these discrepancies.[15,21,35,36] In the next section (Electrokinetic Potential), we will discuss the lack of physical significance of such a specific binding constant.

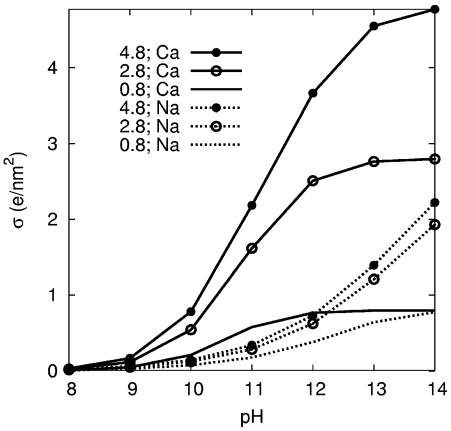

Figure 4. Simulated (GCMC) surface charge density, σ, vs pH for a bulk solution containing either 2 mM calcium (solid lines) or 2 mM sodium (dotted lines) for increasing surface site density: 0.8 (no symbols), 2.8 (empty circles), and 4.8 sites/nm^2 (filled circles).

Obviously, the surface charge density, in absolute value, is significantly higher in the presence of a calcium than of a sodium salt; see Figure 4. In the former case, the surface charge density reaches its maximum value, corresponding to the surface site density, when pH is raised. In the presence of a sodium salt, the same behavior is only observed for low surface site densities. With 2.8 and 4.8 sites/nm^2, the repulsion between sites becomes prohibitively large and the ionization becomes saturated. Indeed, almost the same surface charge density is found for these two surface site densities.

The reduction of α as the 1:1 salt concentration goes down can be seen in Figure 5. A similar behavior is found as in Figure 2. Again, the deprotonation of surface sites is hindered by the electrostatic repulsion with their ionized neighbors, which results in a flattening of the titration curves. It should be noted, that whereas the increase in electrostatic repulsions (responsible for the decrease in α) in Figure 2 is the result of the shortening of the lattice parameter, in Figure 5, it is the result of a reduced electrostatic screening.

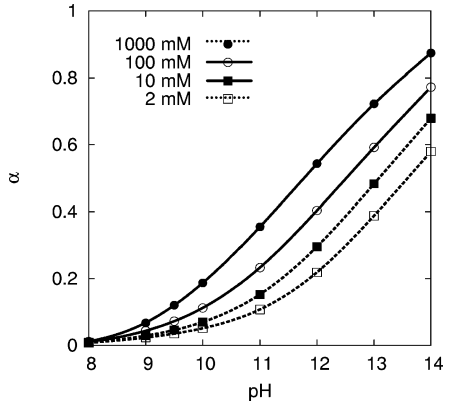

Figure 5. Simulated (GCMC) ionization fraction, α, vs pH for a surface in contact with a bulk solution containing a sodium 1:1 electrolyte at various concentrations: (solid line and filled circles) 1000 mM NaX, (solid line with empty circles) 100 mM NaX, (dashed line with filled squares) 10 mM NaX, and (dashed line with empty squares) 2 mM NaX.

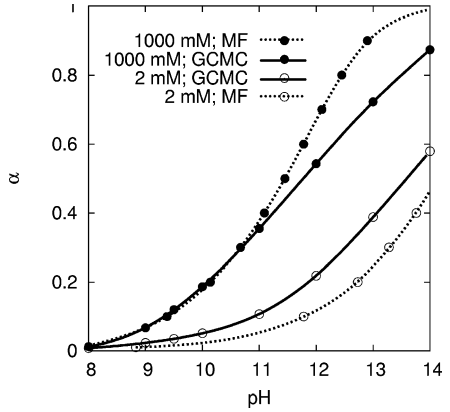

Figure 6. Simulated (GCMC) (solid lines) and calculated through the mean field theory (MF) (dotted lines) ionization fraction, α, vs pH for a surface in contact with a bulk solution containing a sodium 1:1 electrolyte at two concentrations: (filled circles) 1000 mM NaX and (empty circles) 2 mM NaX.

The general behavior depicted in Figures 2 and 5 can be found already with the mean field theory. As an example, the titration curves obtained through the classical theory are given in Figure 6. However, the GCMC and mean field theory values of the ionization fraction of surface sites are far from being equal. The ionization fraction appears in Figure 6 as a function of pH and shows that, at 2 mM, the mean field theory lies well below GCMC predictions. This discrepancy increases with pH. It is the replacement of the potential of mean force between an ion and the wall by the mean electrostatic energy, and the neglect of ionic correlations which such a replacement implies,[46,50] that causes the difference.

As the salt concentration is increased to 1000 mM, an opposite behavior is observed. At pH values close to the pK_0 value, for low surface charge, the mean field theory results are in good agreement with GCMC predictions. As the pH and the corresponding surface charge are increased, however, the ion densities near the wall become larger and as a result the excluded volume effect becomes more important, until at pH $\sim$ 11 the mean field theory result lies above the GCMC predictions. Therefore, the shortcomings of the classical theory at high concentration and pH (pH > 11) are due to its neglect of the ionic size and the corresponding hard-core correlations.[47]

These case studies are presented to introduce or recall the basic behavior of a surface titration curve. The mean field theory is able to qualitatively describe, but not quantitatively, the charging of surfaces in solution containing a single salt solution. Below, we will present some cases where the mean field theory becomes inadequate to even qualitatively predict the general charging behavior of dispersion in equilibrium with mixed salt solution.

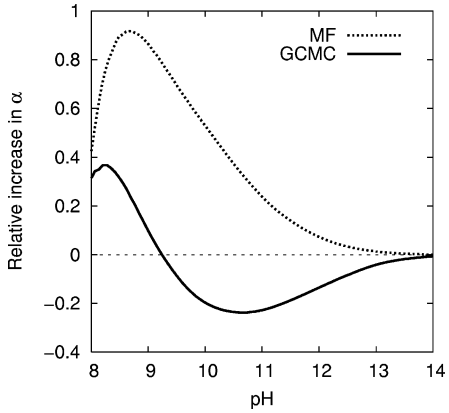

Figure 7. Relative increase in the surface ionization fraction when adding 1000 mM NaX to a bulk solution containing 20 mM CaX_2 at different pH values. The dotted line and the solid line give the results predicted by the mean field theory (MF) and GCMC simulations, respectively.

From the basis of the mean field theory, we would expect a net increase in α as the ionic strength of a 20 mM CaX_2 bulk solution is increased by adding a salt. This is true if the added salt contains a multivalent cation (not shown here). This is also true if a sodium salt is added but only if the solution pH is below the pK_0; see Figure 7. For this pH range, with a low surface charge density, the system behaves classically and the mean field theory predicts an increase in α which reaches a maximum followed by a subsequent decrease in qualitative agreement with the GCMC simulations. As the pH is raised above pK_0, however, a decrease in α (the relative increase in α becomes negative) is observed in the simulations. The mean field theory fails to predict such a behavior: it uniformly predicts a gain in ionization fraction (the relative increase in α is always positive). The latter decreases when pH is raised but remains positive. For example, upon addition of 1000 mM NaX at pH 10.8, the simulations show a decrease in surface charge of 20%, while mean field theory predicts a net increase in the surface charge of more than 30%.

The relative increase in α against pH behavior when adding 1000 mM NaX to a bulk solution containing 20 mM CaX_2 is mainly explained by the competition between calcium and sodium ions in the EDL. The screening by divalent calcium ions is larger than that by sodium ions, thus the surface ionization is higher in the presence of calcium ions, as already shown in Figures 2 and 3. The addition of 1000 mM sodium salt in the bulk leads to the decrease in the concentration of calcium ions and a reduction of α. A decrease in α is observed when pH > pK_0, for example, when the surface charge density is substantial; otherwise, an increase in α is predicted at pH < pK_0 (low surface charge densities), when sodium is the dominating counterion. This is illustrated in Figure 8 where the excess ratio of calcium to sodium counterions in the EDL is plotted against pH.

Figure 8 shows that for both the mean field theory and GCMC an increase in α, found in Figure 7, occurs for a Ca^{ex}/Na^{ex} ratio lower than 0.1, when pH < pK_0. As the pH is raised, less calcium ions are replaced by sodium counterions in the EDL. However, since the mean field theory neglects ion−ion cor-

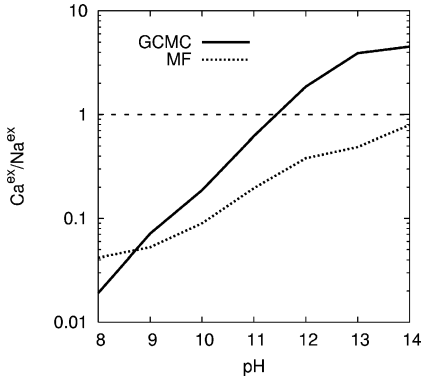

Figure 8. Excess ratio of calcium to sodium counterions against pH found through GCMC simulations and mean field theory calculation (MF). The bulk conditions are the same as those for Figure 7.

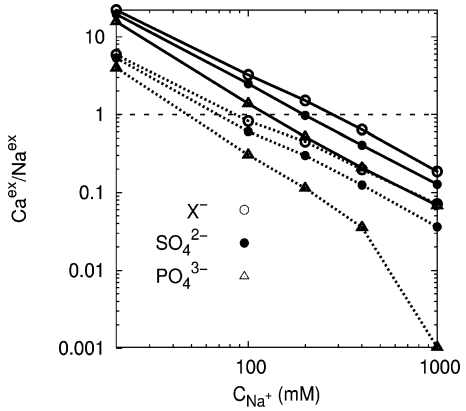

Figure 9. Excess concentration ratio of calcium to sodium counterions vs sodium counterion concentration for a surface in solution of varying bulk conditions at pH 9 (dotted lines) and pH 10 (solid lines). The bulk always contains 20 mM of CaX_2 in addition to sodium salts of varying concentration with different co-ions: X^- (empty circles), SO_4^{2-} (filled circles), and PO_4^{3-} (triangles).

relations, it overestimates the entropy of the EDL and underestimates the calcium accumulation in the vicinity of the surface. In particular, it is unable to predict a Ca^{ex}/Na^{ex} ratio larger than unity. This means that the mean field theory fails to even qualitatively describe the charging behavior of a surface in a salt mixture.

Another example of the competition between sodium and calcium in the EDL and its result on the surface ionization is given in Figures 9 and 10 when sodium salts are gradually added to a bulk solution containing 20 mM CaX_2 at two fixed pH values (pH 9 and 10). These two figures also illustrate the effect of the co-ion valency. A consequence of the successive addition of a sodium salt is that more calcium ions are replaced by sodium in the EDL; see Figure 9. Under these circumstances and for a fixed value of pH, the surface charge of C−S−H decreases, until at an excess ratio in the EDL of unity ($Ca^{ex}/Na^{ex} \approx 1$) a further addition of sodium salt leads to an increase in α.

We note that the decrease in α as a function of sodium salt is also promoted by the co-ion valency; see Figures 10 and 11. That is, a higher valency of the co-ion results in a larger decrease in α. Following our previous discussion, this is not an unexpected finding since multivalent co-ions favor the calcium exchange with sodium in the double layer; see Figure 9 and ref 24.

On the other hand, the accumulation of calcium in the EDL is strengthen by the surface charge. In other words, a huge amount of sodium salt is needed to remove calcium from the EDL at high surface charge values. That is the reason for pH > 10 (almost the pK_0 value), the decrease in α is uniform. As

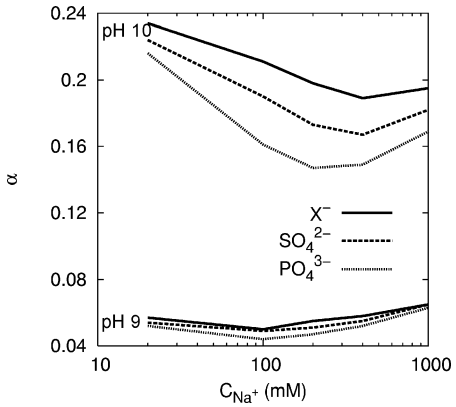

Figure 10. Ionization fraction vs sodium counterion concentration for a surface in solution of varying bulk conditions at pH 9 and pH 10. The bulk always contains 20 mM CaX_2 in addition to sodium salts of varying concentration with different co-ions: X^- (solid lines), SO_4^{2-} (dashed lines), and PO_4^{3-} (small dashed lines).

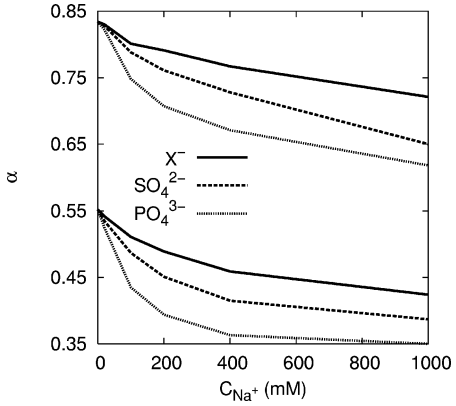

Figure 11. Ionization fraction vs sodium counterion concentration for a surface in solution of varying bulk conditions at pH 11 (lower three curves) and pH 12 (upper three curves). The bulk always contains 20 mM CaX_2 in addition to sodium salts of varying concentration with different co-ions: X^- (solid lines), SO_4^{2-} (dashed lines), and PO_4^{3-} (small dashed lines).

TABLE 1: Operating Conditions for the Titration Experiments

NaOH added (mol)[a]	pH_{eq}[a]	$[Ca^{2+}]_{eq}$ mM[a]	$[Na^+]_{eq}$ mM[a]	Δα no. OH/SiO[b]	Na/SiO[b]
0	10.35	1.310	0.00	0	0.00
5.0×10^{-5}	10.50	1.740	7.40	0.02	0.01
3.0×10^{-4}	10.95	0.400	11.50	0.11	0.04
$6.5\ 10^{-4}$	11.45	0.080	15.30	0.16	0.09
1.35×10^{-3}	12.10	0.006	25.60	0.22	0.18
3.7×10^{-3}	12.65	0.003	74.80	0.17	0.35
1.12×10^{-2}	13.00	0.002	233.2	X	0.54

[a] The first column indicates the amount of added NaOH, the second the solution pH at equilibrium, and the third and fourth the calcium and sodium equilibrium concentration in the supernatant expressed in mM, respectively. [b] The two last columns give the amount of hydroxide ions consumed (OH/SiO) and the excess amount of sodium accumulated in the EDL (Na/SiO) per silanol site, respectively.

an example, in Figure 11, α is plotted against the bulk sodium salt concentration at pH 11 and pH 12.

3.1.2. Comparison between Experiment and Simulation Results. GCMC simulations were performed under the same conditions (pH, ion concentrations, temperature, etc.) as in the experiments. That is, the pH and ion concentrations used in the simulations were those measured at equilibrium (Table 1). Under these circumstances, the excess amount of sodium ions found in the EDL through simulations was simply the one thought to

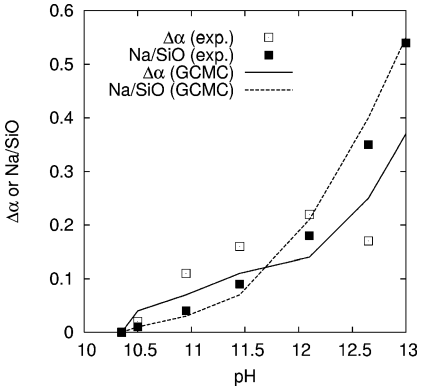

Figure 12. Comparison between simulated (curves) and experimental (points) net increase of ionization fraction ($\Delta\alpha$) and sodium counterion "adsorption" (Na/SiO) of C−S−H nanoparticles dispersed in solutions containing a low calcium concentration; see Table 1 for more details. Filled squares and dashed curves give an excess amount of sodium incorporated in the EDL at the interface between C−S−H particles and solution. The latter is expressed in terms of the ratio of sodium to silanol group amount. Open squares and the solid curve give the net increase of surface ionization fraction ($\Delta\alpha$) found through titration experiments and simulations, respectively.

be comparable with experiments, for example, the quantity of sodium ions disappearing from the bulk solution after the addition of NaOH. Figure 12 shows the evolution, against pH, of the net increase in ionization fraction and Na/SiO from both experiments and GCMC simulations.

As mentioned before, C−S−H dispersions were chosen to contain a small amount of calcium ions (see Table 1), but even under this condition, one can observe, in Figure 12, a nonnegligible discrepancy between the net increase in C−S−H surface charge and the corresponding amount of sodium incorporated in the EDL. Indeed, in absence of calcium ions, one should find an equality between $\Delta\alpha$ and Na/SiO. That is, the excess amount of sodium ions found should exactly compensate for the number of ionized sites. Two distinctive zones in pH are found delimited by a pH value of 12. Below pH 12, $\Delta\alpha$ lies above Na/SiO. Here, the calcium ions are still playing an important role in neutralizing the C−S−H surface charge (see the third and fourth columns of Table 1). As pH is increased, however, the bulk calcium concentration drops (see Table 1) due to an additional precipitation of C−S−H and becomes negligible compared with that of sodium; as a result, more calcium counterions in the EDL are exchanged by sodium, with the latter becoming the unique counterion, until at pH > 12 $\Delta\alpha$ lies below Na/SiO.

The simulated and experimental results of $\Delta\alpha$ and Na/SiO are in good agreement; see Figure 12. For the Na/SiO results, the observed and predicted values are within 0.05 units. For $\Delta\alpha$, the agreement is still good: a crossover of $\Delta\alpha$ and Na/SiO is predicted to occur 0.5 pH unit lower than what was observed in experiments. Because of the high experimental uncertainties in $\Delta\alpha$ when pH > 12, one should interpret the experimental $\Delta\alpha$ with caution in this pH range. Taking these uncertainties into consideration, we can still conclude that GCMC simulations are able to predict the difference observed between $\Delta\alpha$ and Na/SiO. This indicates that our theoretical model is capable of reproducing electrostatic effects that cause the titration of the individual silanol groups of C−S−H nanoparticles leading to the macroscopic and observable surface charge and ion "adsorption".

3.2. Electrokinetic Potential. Electrokinetic measurements of the C−S−H dispersions have also been conducted under various conditions to test the validity of our model for the C−S−H surface charge. Indeed, the electrokinetic behavior of C−S−H particles can give a valuable indication of their surface charge state.

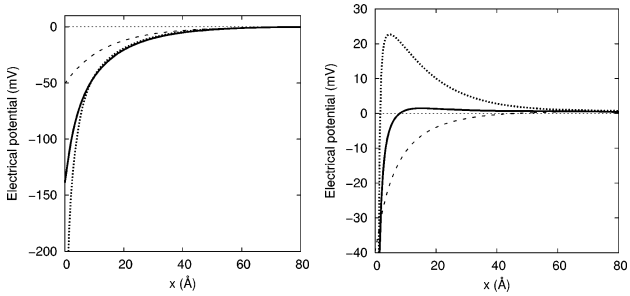

Figure 13. Electrical potential profile as a function of the distance normal to the surface (x) for varying bulk conditions and increasing pH values: pH 9 (dashed line), pH 11 (solid line), and pH 14 (dotted line). (a) Surface next to a bulk solution containing 40 mM NaX. (b) Surface next to a bulk solution containing 20 mM CaX_2.

Initially, we would like to present some simulation results. They are not intended as an exhaustive study of the electrokinetic potential but rather as an introduction to the electrokinetic experiments performed on C−S−H.

3.2.1. Simulation Results. It has already been shown by Monte Carlo simulations,[2,4−8,11−22,14,22,51] and accurate analytical theories,[1,3,9,10,12,23,24] that a charge reversal can take place in an electric double layer under some specific conditions. In particular, it can happen for highly coupled systems, that is, highly charged surfaces next to electrolyte solutions containing multivalent counterions. Since the energy of the system is lowered by a packing of ions near the wall, highly charged colloidal particles accumulate their counterions in a thin layer near the surface. At finite electrolyte concentration, the accumulation can more than simply neutralize the surface charge. Under these circumstances and at a certain distance from the surface, the apparent charge of particles appears to be reversed compared with its formal charge, σ_0. The ion−ion correlations are known to be responsible for this phenomenon.

In Figure 13, the electrostatic profile corresponding to a surface next to a bulk electrolyte solution containing either 40 mM NaX (Figure 13a) or 20 mM CaX_2 (Figure 13b) for varying pH values (or surface charge density) is plotted. As can be seen, nonmonotonic profiles occur for surfaces at a sufficiently large surface charge density (or pH value) in contact with a solution containing divalent calcium counterions. What is more, a positive electrostatic potential is found near a negatively charged surface. A test ion would therefore feel an electrostatic potential whose sign is opposite to the expected one. Consequently, for such conditions, a reversal of the electrokinetic potential measured through electrophoretic measurements is also expected; see Figure 13b. Conversely, monotonic profiles of the electrostatic potential are found, even for high pH or surface charge density, for surfaces in equilibrium with bulk solution containing monovalent counterions; see Figure 13a. This is in line with the previous discussion where we pointed out that overcharging predominantly occurs for systems containing multivalent counterions. It should be stressed however that charge reversal can also be predicted for surfaces in contact with a reservoir containing only monovalent counterions but only for nonphysical surface charge densities.

As the counterion size is raised and for high pH (or surface charge), the hard-core correlation increases, and as a result, the overcharging decreases dramatically. For a counterion size of 6 Å, it has disappeared completely. This is shown by the series of results at a concentration of 20 mM CaX_2 and increasing pH

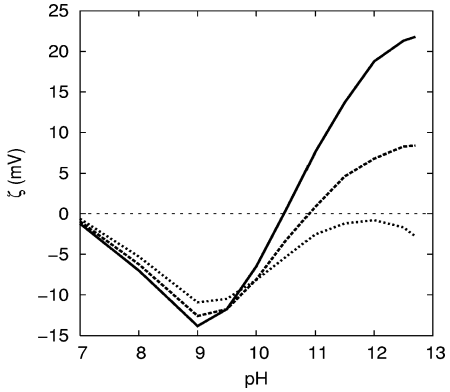

Figure 14. Simulated ζ potential as a function of solution pH of a surface next to a bulk solution containing 20 mM CaX_2 by varying the calcium ion size. The calcium ion diameters shown are equal to 4 Å (solid line), 5 Å (dashed line), and 6 Å (dotted line), while that of X^- is maintained to 4 Å.

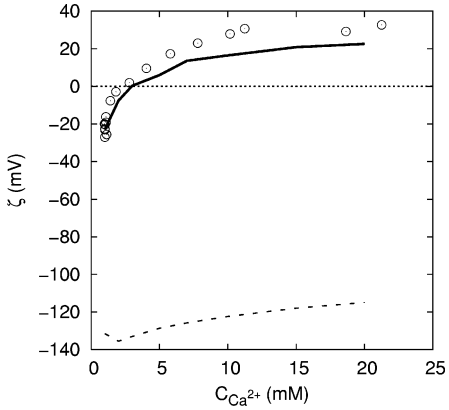

Figure 15. Simulated (solid curve) and experimental (empty circles) ζ potential against calcium concentration for a C−S−H dispersion in pure $Ca(OH)_2$ solutions. The results of the mean field theory (dashed curve) are given for comparison.

values in Figure 14. This observation has also been made recently by Quesada-Pérez et al.[52] but in a restricted PM taking a constant surface charge density. One could also note that for the lowest pH studied the opposite takes place, that is, the hard-core correlation leads to an increase of ζ. This is also in qualitative agreement with previous works.[22,26] The rise of the hard-core correlation which leads to the decrease in the overcharging can be schematically understood in terms of counterion covering surface area (projection of the counterion cross-section) per surface site area (4.56 Å × 4.56 Å). For a counterion size of 4 Å, the covering surface area per surface site area is 60%; for 5 Å, it reaches 94%; for 6 Å, it would be 136%. The last two values are not physically possible: the maximum value is 78%. Besides, the increase in counterion size leads to the decrease in the screening of the ionized surface sites and the subsequent decrease in the surface charge.

Obviously, there is a competition between electrostatic and hard-core correlations. When the latter dominates, there will be no charge reversal in the EDL. This result should not be taken too seriously. At high densities, the hard core becomes a parameter that tends to "incorporate" several shortcomings of the dielectric continuum model. For example, it is known that the incorporation of explicit solvent molecules induces fast screening and increases the accumulation of ions in the vicinity of charged/uncharged walls.[25,53,54] The best conclusion to be drawn from Figure 14 and, for example, the previous work on surface forces by Kekicheff et al.,[10] is that caution should be exercised when the hard-core size becomes an important parameter.

3.2.2. Comparison between Experiment and Simulation Results. As pointed out above, in the case of highly charged C−S−H particles and divalent calcium ions, electrokinetic measurements should provide experimental evidence for the reversal of the so-called ζ potential (approximately equal to the diffuse potential). Mobility reversal was already observed several decades ago for certain polyelectrolytes in solutions of divalent counterions[15] and for colloidal dispersions in solutions of tri- and tetravalent counterions.[16] More recently, mobility reversals of different types of colloids have also been reported in 2:1 and 3:1 electrolytes.[17,20] Charge reversal was also reported for mica surfaces in a 2:1 calcium electrolyte observed through streaming potential measurements[21] and deduced from surface force apparatus measurements.[14] Unfortunately, results such as these were traditionally interpreted in the framework of mean field theory, except in ref 14, and the charge reversal was explained by specific chemical adsorption of multivalent counterions.

To our knowledge, only the group of Lozada-Cassou have put some efforts into describing the electrokinetic potential determined through electrophoretic mobility (μ_e) by developing a new theoretical approach,[22,26] called primitive model electrophoresis, where the ionic correlation mechanism was considered in some detail. In particular, Lozada-Cassou et al. have shown several shortcomings of the classical theory of Wiersema, O'Brien, and White[55] relevant for a highly coupled system where a mobility reversal is predicted in agreement with the previous results present in Figure 14.

Figure 15 shows the ζ potential deduced from electrophoretic measurements of C−S−H dispersions in $Ca(OH)_2$ solutions for different concentrations compared with that obtained from simulation and the mean field theory. The ζ potential of C−S−H particles is found to rise continuously together with pH and calcium concentration from negative values, at low calcium concentrations, to positive values, for the high calcium concentration. The sign reversal of the ζ potential is found for a calcium concentration of approximately 2 mM. Our simulations allow us to quantitatively describe this electrokinetic behavior. On the contrary, the mean field theory completely fails to explain the ζ potential reversal observed. In light of these results, two conclusions can be made. First, physical interactions alone explain the sign reversal of the electrokinetic potential. Consequently, the C−S−H charge reversal is apparent, for example, it does not reflect a sign reversal of the mineral itself but originates from ionic correlations leading to a strong accumulation of calcium counterions in the vicinity of the surface of C−S−H particles. Second, the specific adsorption constant traditionally used to justify charge reversal in the framework of the mean field theory does not appear to have a real physical meaning. It is only a fitting parameter in the mean field approach. Attard[6,25] and Ennis and Kjellander[7] have shown why the PB equation often succeeds in fitting experimental data but giving *effective* parameters. This is based on the fact that the qualitative exponential decay of the potential and ion density in the EDL at a rate approximately equal to the Debye length is correct. In addition, they have given numeric results together with a comprehensive theoretical development that relates the *effective* surface charge that appears in the PB theory to the bare surface charge density of the system.

Figure 16 shows the simulated and experimental electrokinetic behavior of C−S−H particle dispersions in solutions by varying the 2:1 calcium electrolyte concentration and adjusting the pH at two distinct values by the addition of NaOH. The electrokinetic potential for C−S−H dispersions in pure $Ca(OH)_2$ solution

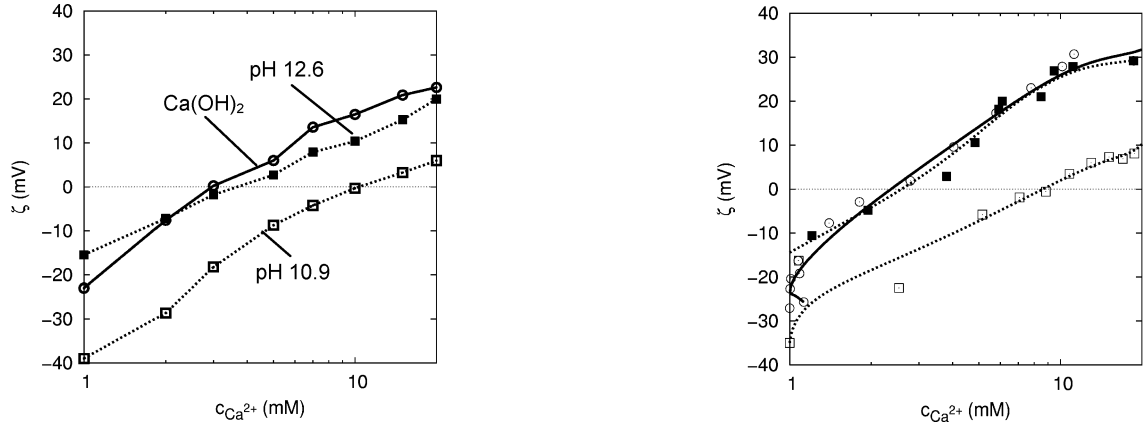

Figure 16. ζ potential against calcium concentration for pure $Ca(OH)_2$ solutions (solid line, empty circles) and two fixed bulk pH values: pH 10.9 (dotted line, empty squares) and pH 12.6 (dotted line, filled squares). The calcium concentration and solution pH were adjusted by adding $CaCl_2$ and NaOH to C−S−H dispersions in $Ca(OH)_2$ solution. (a) Curves calculated from GCMC simulations. (b) Experimental ζ potential deduced from electrophoretic mobility.

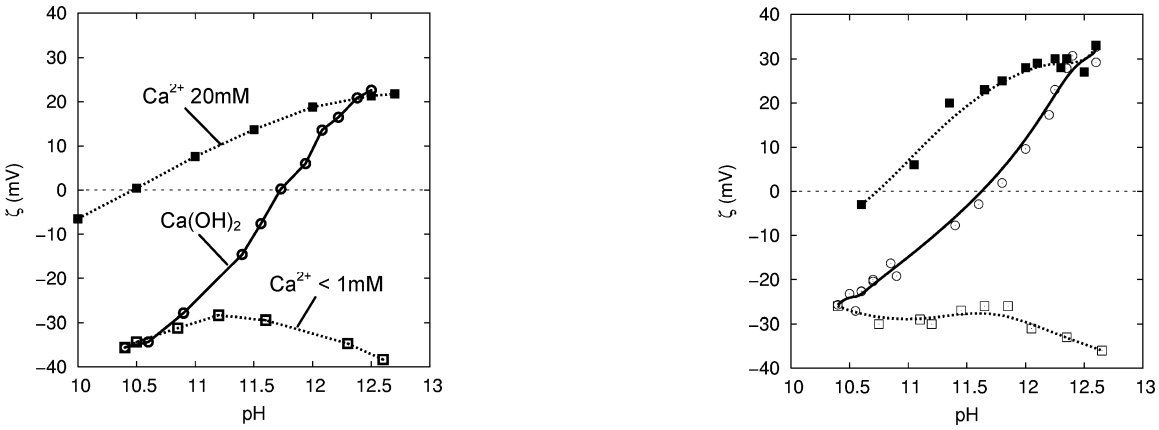

Figure 17. Simulated (a) and experimental (b) ζ potential against bulk solution pH for varying bulk conditions. Bulk conditions are either pure $Ca(OH)_2$ solution (empty circles, solid line), less than 1 mM calcium 2:1 electrolyte in addition to various amounts of NaOH (empty squares, dotted line), 20 mM calcium from a mix of $CaCl_2$ and $Ca(OH)_2$ salt solution (filled squares, dotted line).

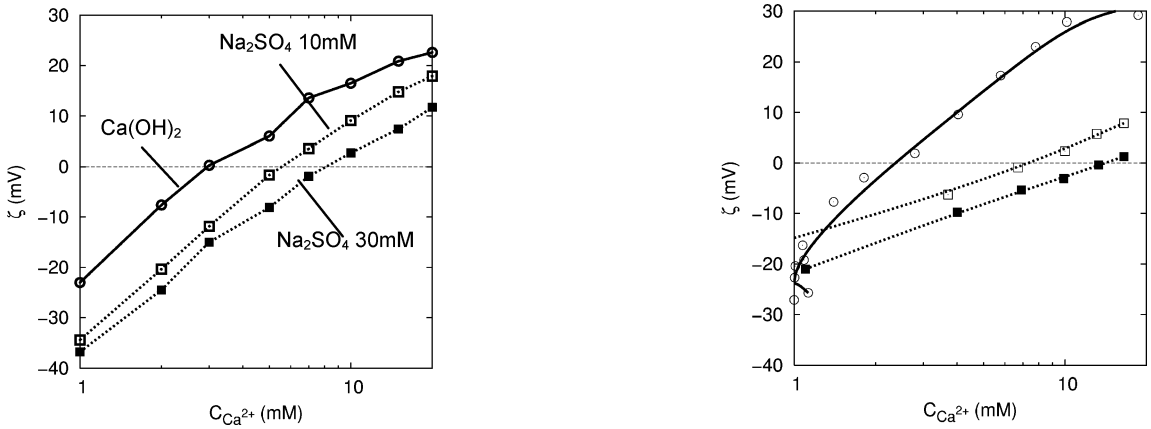

Figure 18. Simulated (a) and experimental (b) ζ potential against bulk calcium concentration for varying bulk conditions. Bulk conditions are either pure $Ca(OH)_2$ solutions (empty circles, solid line), 10 mM Na_2SO_4 in addition to various amounts of $Ca(OH)_2$ (empty squares, dotted line), 30 mM Na_2SO_4 in addition to various amounts of $Ca(OH)_2$ (filled squares, dotted line).

is also plotted for comparison. A shift of the isoelectric point toward higher calcium counterion concentration is observed when the pH of C−S−H dispersions is lowered in agreement with the simulation predictions. That is, the overcharging drops dramatically when pH and consequently the surface charge is diminished. In that case, a much higher calcium concentration is needed to regain a sign reversal of the ζ potential and the corresponding apparent charge reversal. By comparing mobility results of C−S−H dispersions in pure $Ca(OH)_2$ solutions ($Ca(OH)_2$ curve) and the ones just studied (pH 12.6 and pH 10.9 curves), one can also see that the pH 12.6 curve lies below the $Ca(OH)_2$ curve. Again, this behavior is well explained by ionic correlations. Indeed, the addition of monovalent Na^+ ions induces a decrease in ionic correlations that disfavor the accumulation of calcium counterions in the vicinity of C−S−H particles.

Instead of studying the electrokinetic behavior of C−S−H dispersions in electrolyte solution by varying the calcium concentration and setting pH values, one could also set the calcium concentration and vary the solution pH. This is shown

in Figure 17 where the dispersions were chosen to be in equilibrium with a salt solution containing either 20 mM or less than 1 mM calcium. The calcium concentration and pH of solutions of C−S−H dispersions are adjusted to the desired value by adding $CaCl_2$ and NaOH salts, respectively. The electrokinetic potential for C−S−H dispersions in pure $Ca(OH)_2$ solution is also plotted for comparison. The decrease of calcium concentration from 20 to lower than 1 mM results in a large decrease of the electrokinetic potential. Furthermore, for the lower calcium concentration (below 1 mM), no ζ potential or apparent charge reversal can be observed as predicted by simulations.

Figure 18 shows how the ζ potential is reduced when adding Na_2SO_4 salt to dispersions in $Ca(OH)_2$ solutions. It is again in agreement with the simulation predictions since, as it has already been demonstrated,[24] the surface charge reversal induced by ion−ion correlations is reduced by the addition of monovalent counterions and eventually disappears. The reduction or the disappearance is also known to be promoted by the addition of sodium salt with multivalent anions. Indeed, they are expelled from the EDL compared with the monovalent ones and lead to a lower surface charge density; see the previous section. But, the experimental and simulation ζ potentials exhibit a sign reversal at the highest $Ca(OH)_2$ concentrations even for an addition of 30 mM Na_2SO_4.

This result clearly demonstrates that C−S−H particles possess a strong negatively charged surface, and it makes C−S−H an interesting colloidal particle for not only technical but also theoretical studies.

4. Conclusion

We have reported results from grand canonical Monte Carlo simulations of the surface charge density and electrokinetic behavior of highly charged minerals for varying bulk conditions. Various experiments have been conducted on C−S−H particles, which are the main ingredient in cement paste, to test the validity of our model and simulations. The simulation and experimental results have been compared with the mean field theory predictions. In the simulations, we have used the primitive model, where all ions are treated explicitly, while water only enters as a continuum characterized by its relative dielectric permittivity. The C−S−H surface has been modeled as a lattice with explicit ionizable sites, mimicking the protonation and deprotonation of silanol groups by the use of one p*K* value. In this theoretical approach, in addition to the knowledge of the surface site density, just one p*K* value is needed to calculate the charging behavior of a mineral.

The comparison of experimental and simulation results shows that the Coulombic interaction between the charged species is the main factor that determines the charging (titration) and electrokinetic behavior of C−S−H. The excellent agreement between experimental and simulated results, both with respect to surface titration and electrokinetic behavior, confirms that the dielectric continuum model has a sound physical basis. The agreement extends over a wide range of electrostatic coupling, from a weakly charged surface with mainly monovalent counterions to a highly charged one with divalent counterions.

The mean field theory shows a qualitative agreement with simulations for systems containing monovalent counterions. It fails qualitatively, however, to predict the charging behavior of a dispersion in a mixture of monovalent and divalent counterions. For example, the mean field theory predicts a pronounced increase in the surface charge density when adding a sodium ion to a C−S−H dispersion with divalent calcium ions, while Monte Carlo simulations predict the opposite. The mean field theory also strongly underestimates the surface charge density for a particle dispersion with divalent counterions. We conclude that the mean field theory cannot be used to describe the charging behavior for strongly coupled systems, that is, in solutions with divalent or multivalent ions, high electrolyte concentration, and/or high surface charge density.

The excellent agreement between experimental and simulated electrokinetic potential under various conditions clearly demonstrates that the charge reversal of C−S−H particles is apparent. The simulations show that the accumulation of calcium ions can lead to an overcompensation of the negative C−S−H surface charge when ion−ion correlations are strong. The apparent charge reversal occurs at high pH and calcium concentrations as shown by both experiment and simulations. Thus, we can conclude that the concept of "specific binding" traditionally introduced in the classical mean field theory appears to act as a fitting parameter without a physical basis. Finally, we note that the addition of a salt containing monovalent counterions, for example, Na_2SO_4, reduces the apparent charge reversal. For sufficiently large additions of sodium sulfate, or any other sodium salt, the charge reversal will disappear.

Here, we have investigated the charging and electrophoretic properties of C−S−H in a dilute suspension. In a more concentrated suspension, the interaction between the particles will affect these properties. That is, the concentration of the suspension will influence the surface charge of the particles as well as the force between them. We will return to this problem in a future communication.

Acknowledgment. A generous grant from the CNRS and the Swedish Foundation for Strategic Research is gratefully acknowledged. We also acknowledge the support of the CRI from the University of Bourgogne and the CINES (France) for access to their computer facilities.

References and Notes

(1) Van Megen, W.; Snook, I. *J. Chem. Phys.* **1980**, *73*, 4657.
(2) Bhuiyan, L. B.; Outwiate, C. W.; Levine, S. *Mol. Phys.* **1981**, *42*, 1271.
(3) Valleau, J. P.; Torrie, G. M. *J. Phys. Chem.* **1982**, *86*, 3251.
(4) Attard, P.; Mitchell, D. J.; Ninham, B. W. *J. Chem. Phys.* **1988**, *89*, 4358.
(5) Mier-yTeran, L.; Suh, S. H.; White, H. S.; Davis, H. T. H. *J. Chem. Phys.* **1990**, *92*, 5087.
(6) Attard, P. *J. Phys. Chem.* **1995**, *99*, 14174.
(7) Ennis, J.; Marcelja, S.; Kjellader, R. *Electrochim. Acta* **1996**, 2115.
(8) Greberg, H.; Kjellander, R. *J. Chem. Phys.* **1998**, *108*, 2940.
(9) Sjöström, L.; Åkesson, T.; Jönsson, B. *Ber. Bunsen-Ges. Phys. Chem.* **1996**, *100*, 889.
(10) Guldbrand, L.; Jönsson, B.; Wennerström, H.; Linse, P. *J. Chem. Phys.* **1984**, *80*, 2221.
(11) Kjellander, R.; Marcelja, S. *Chem. Phys. Lett.* **1984**, *112*, 49.
(12) Kjellander, R.; Åkesson, T.; Jönsson, B.; Marcelja, S. *J. Chem. Phys.* **1992**, *97*, 1424.
(13) Decker, G. *Science* **1997**, *82*, 215.
(14) Kekicheff, P.; Marcelja, S.; Senden, T. J.; Shubin, V. E. *J. Chem. Phys.* **1993**, *99*, 6098.
(15) Strauss, U. P.; Gershfeld, N. L.; Spiera, H. *J. Am. Chem. Soc.* **1954**, *76*, 5909.
(16) Ottewill, R. H.; Shaw, J. N. *J. Colloid Interface Sci.* **1968**, *26*, 110.
(17) Elimelech, M.; O'Melia, C. R. *Colloids Surf.* **1990**, *44*, 165.
(18) Besteman, K.; Zevenbergen, M. A. G.; Heering, H. A.; Lemay, S. G. *Phys. Rev. Lett.* **2004**, *93*, 802.
(19) Plassard, C.; Lesniewska, E.; Pochard, I.; Nonat, A. *Langmuir* **2005**, *21*, 7263.
(20) Nachbaur, L.; Nkinamubanzi, P. C.; Nonat, A.; Mutin, J. C. *J. Colloid Interface Sci.* **1998**, *202*, 261.
(21) Scales, P. J. *Langmuir* **1990**, *6*, 582.
(22) Lozada-Cassou, M.; Gonzales-Tovar, E.; Olivares, W. *Phys. Rev. E* **1999**, *60*, R17.

(23) Jönsson, B.; Wennerström, H.; Nonat, A.; Cabane, B. *Langmuir* **2004**, *20*, 6702.
(24) Jönsson, B.; Nonat, A.; Labbez, C.; Cabane, B.; Wennerström, H. *Langmuir* **2005**, *21*, 9211.
(25) Attard, P. *Adv. Chem. Phys.* **1996**, *92*, 1.
(26) Quesada-Perez, M.; Gonzalez-Tovar, E.; Martin-Molina, A.; Lozada-Cassou, M.; Hidalgo-Alvarez, R. *ChemPhysChem* **2003**, *4*, 235.
(27) C═CaO, S═SiO_2, and H═H_2O in the cement chemistry notation.
(28) Cong, X.; Kirkpatrick, R. J. *J. Am. Ceram. Soc.* **1996**, *79*, 1585.
(29) Damidot, D.; Nonat, A.; Barret, P.; Bertrandie, P.; Zanni, H.; Rassem, R. *Adv. Cem. Res.* **1995**, *7*, 1.
(30) Plassard, C.; Lesniewska, E.; Pochard, I.; Nonat, A. *Ultramicroscopy* **2004**, *100*, 331.
(31) Ray, N. H.; Plaisted, R. J. *J. Chem. Soc., Dalton Trans.* **1983**, 475.
(32) Svensson, I. L.; Sjöberg, S.; Öhman, L.-O. *J. Chem. Soc., Faraday Trans.* **1986**, *82*, 3635.
(33) Tanford, C.; Kirkwood, J. G. *J. Am. Chem. Soc.* **1957**, *79*, 5333.
(34) Borkovec, M.; Koper, G. J. M. *Macromolecules* **1997**, *30*, 2151−2158.
(35) Yates, D. E.; Levine, S. L.; Healy, T. W. *J. Chem. Soc., Faraday Trans. 1* **1974**, *70*, 1807.
(36) Davis, J. A.; James, R. O.; Leckie, J. O. *J. Colloid Interface Sci.* **1977**, *63*, 480.
(37) Hiemstra, T.; Van Riemsdijk, W. H.; Bolt, G. H. *J. Colloid Interface Sci.* **1989**, *133*, 91.
(38) Borkovec, M. *Langmuir* **1997**, *13*, 2608.
(39) Roller, P. S.; Erwin, G. *J. Am. Chem. Soc.* **1940**, *62*, 461.
(40) Hunter, R. J.; White, L. R. *Foundations of Colloid Science*; Clarendon Press: Oxford, U.K., 1995.
(41) Plassard, C.; Labbez, C.; Pochard, I.; Lesniewska, E.; Nonat, A. *Ceramics* **2005**, in press.
(42) Lund, M.; Jönsson, B.; Pederson, T. *Mar. Chem.* **2003**, *80*, 95.
(43) Valleau, J. P.; Cohen, L. K. *J. Chem. Phys.* **1980**, *72*, 5935.
(44) Metropolis, N. A.; Rosenbluth, A. W.; Rosenbluth, M. N.; Teller, A.; Teller, E. *J. Chem. Phys.* **1953**, *21*, 1087.
(45) Widom, B. J. *Chem. Phys.* **1963**, *39*, 2808.
(46) Svensson, B. R.; Woodward, C. E. *Mol. Phys.* **1988**, *64*, 247.
(47) Torrie, G. M.; Valleau, J. P. *J. Chem. Phys.* **1980**, *73*, 5807.
(48) Kesvatera, T.; Jönsson, B.; Thulin, E.; Linse, S. *Proteins* **1997**, *37*, 106.
(49) Valisko, M.; Henderson, D.; Boda, D. *J. Phys. Chem. B* **2004**, *108*, 16548.
(50) Jönsson, B.; Wennerström, H.; Halle, B. *J. Chem. Phys.* **1980**, *84*, 2179.
(51) Henderson, D.; Blum, L.; Smith, W. R. *Chem. Phys. Lett.* **1979**, *63*, 381.
(52) Quesada-Perez, M.; Martin-Molina, A.; Hidalgo-Alvarez, R. *J. Chem. Phys.* **2004**, *121*, 8618.
(53) Spohr, E. *Electrochim. Acta* **2003**, *49*, 23.
(54) Torrie, G. M.; Kusalik, P. G.; Patey, G. N. *J. Chem. Phys.* **1989**, *90*, 4513.
(55) O'Brien, R. W.; White, L. R. *J. Chem. Soc., Faraday Trans. 2* **1978**, *74*, 1607.